Contents lists available at ScienceDirect

Heliyon

Prediction of condylar movement envelope surface based on facial morphology

Kenan Chen [a], Zhehao Zhang [c], Junqi Jiang [a], Junlin Wang [a], Jing Wang [a], Yuchun Sun [b], Xiangliang Xu [a,*], Chuanbin Guo [a]

[a] Department of Oral and Maxillofacial Surgery, Peking University School and Hospital of Stomatology, National Center of Stomatology, National Clinical Research Center for Oral Diseases, National Engineering Research Center of Oral Biomaterials and Digital Medical Devices, Beijing Key Laboratory of Digital Stomatology, Research Center of Engineering and Technology for Computerized Dentistry Ministry of Health, NMPA Key Laboratory for Dental Materials, Beijing, PR China
[b] Center of Digital Dentistry, Faculty of Prosthodontics, Peking University School and Hospital of Stomatology, National Center of Stomatology, National Clinical Research Center for Oral Diseases, National Engineering Research Center of Oral Biomaterials and Digital Medical Devices, Beijing Key Laboratory for Dental Materials, Beijing, PR China
[c] State Key Laboratory of Tribology, Tsinghua University, Beijing, 100084, PR China

ARTICLE INFO

ABSTRACT

The present study aimed to predict the envelope surfaces from facial morphology. Condylar envelope surfaces for 34 healthy adults were formed and simplified as sagittal section curves. Cephalometric and maximum mandibular moving distances measurement were performed on the participants. There was no statistically significant difference (p = 0.763) between the left and right maximum lateral movements. There was a statistically significant difference in the mandibular body length between the sexes. The envelope surfaces were divided into type 1 with $H_{p2} \geq 1/3\ H_{p1}$ and type 2 with $H_{p2} < 1/3 \times H_{p1}$. SNA and SNB for type 2 were significantly greater than those for type 1 (p < 0.001). Therefore, the participants were divided into four groups based on gender and envelope surface morphology. The curves could be fitted using the second-order Fourier function (R-square ≥0.95). Six facial parameters were selected and a matrix was used to map facial morphology to the envelope surface. Individual sagittal curves were predicted using the matrix and facial parameters, and the envelope surface was predicted using the curve and the condyle model. Deviation analysis for the predicted envelope surface using the actual envelope as a reference was carried out (root mean square = 0.9970 mm ± 0.2918 mm). This method may lay a foundation for the geometric design of artificial fossa components of temporomandibular joint replacement systems. It may improve prosthesis design without flexible tissue repair and guide the movement of the artificial joint head.

1. Introduction

Temporomandibular joint (TMJ) is a complex joint of the human body, which includes the mandibular condyle, facet, disc, and ligament. TMJ movement is affected by its anatomical structure and the occlusal relationship. The concept of orofacial system has been

---

proposed to explain the complexity of TMJ movement [1]. Although TMJ movement cannot be observed directly, advancements in acquisition equipment and computers have allowed accurate, quantitative measurement of mandibular movements [2–9]. Several mathematical models and functional expressions have been established for the movement trajectory [10,11], establishing the future role of artificial intelligence in the medical field. Previous studies of the mandibular condylar process have investigated the range using condylar landmarks, but differences in landmark selection prevent the comparison of these results [12,13]. Besides, this method does not reflect the three-dimensional (3D) shape of the condylar process. We developed a method to analyze condylar movements in four dimensions using cone-beam computed tomography (CBCT) and movement recording data, with the conception of the condyle envelope surface, but this method requires further investigation [14].

Disturbances in the self-restoration of TMJ can lead to temporomandibular disorder (TMD), which causes pain, clicking, muscle tenderness, and limitation of mouth opening [15–18]. Although many researchers have investigated the TMJ through basic research and aimed to find end-stage options [19], there were few practically applicable results. Total TMJ replacement (TMJR) is a biomechanical treatment option for patients with end-stage TMJ disease [20–22]. The artificial TMJR system includes fossa and condyle components, but lacks the disc. The ideal total joint reconstruction should closely mimic the function of the original joint. There are two common TMJR systems available, standardized and personalized systems. Zimmer Biomet and TMJ Concepts have been approved by the United States Food and Drug Administration [23]. At present, there is no gold standard for the artificial TMJR systems. The ball-socket design is the most widely used type. Anatomically, the joint fossa is much larger than the condylar process, making the TMJ movement more flexible. The ball-socket design changes the action curve and limits the condylar movement. It has been demonstrated that the mandibular movements after TMJR are not ideal [24]. Postoperative follow-up of the existing total joint prostheses has revealed limited mandibular movements, with little translational movement of the joint head [25]. After unilateral joint replacement, maximum mouth opening is achieved with significant lateral deviation toward the implanted side [26] and increased load and displacement on the contralateral joint [24,27,28]. The importance of designing a fossa component that acts as a mechanical constraint and guide has been emphasized [29,30]. The envelope surface formed by condylar movement may improve the geometric design of the artificial fossa.

Since end-stage TMD patients are unable to perform normal mandibular movements, the prediction of condylar movements is necessary. A statistical correlation between facial morphology and jaw movements has been reported in several studies [31–34]. Changes in mandibular movements after orthognathic surgery also indicate that facial morphology affects mandibular movements [35, 36].

In this study, the condyle movement envelope surfaces and facial parameters for healthy adults were obtained. The envelope surfaces were simplified as sagittal section curves expressed by mathematical function, and classified according to the morphology. A method was proposed for predicting the shape of condyle movement envelope surfaces, based on the facial morphology and its effectiveness was verified. This study may improve the analysis of condylar movements and the design of the functional surfaces of artificial TMJ fossa.

2. Materials and Methods

2.1. Subjects

This study was approved by the Bioethics Committee of Peking University School and Hospital of Stomatology, Beijing, China (No. Pkussirb-201947091). The inclusion criteria were: (1) no systemic diseases; (2) no facial asymmetry; (3) no history of maxillofacial trauma or surgery; (4) no orthodontic treatment history; (5) no history of TMJ discomfort (pain, clicking, or limited mouth opening) or treatment; (6) no abnormal habits (bruxism or clenching); and (7) complete dentition with a class I occlusal relationship.

Each participant was clinically examined by three trained doctors independently. TMJ clicking, pain or restriction on opening, obvious deviation, and abnormal movements were recorded. Informed consent was obtained from all participants.

2.2. Acquiring the envelope surface for condyle movement

The participants underwent skull and mandible CBCT (NewTom VG, NewTom, Italy; voxel size = 0.3 mm, field of view = 16×16 cm) in the maximum intercuspal position (ICP). The maxilla and mandible were separated in ProPlan CMF 3.0 (Materialise, Belgium) and reconstructed as 3D models with the data obtained by CBCT.

The 3D morphological data and positional relationships between the upper and lower dentition were obtained in the ICP using the TRIOS 3 intraoral scanner (3Shape TRIOS A/S, Copenhagen, Denmark). Two splints were created to attach the anterior teeth in Geomagic Studio 2012 (3D Systems, Rock Hill, SC, USA) and printed using a 3D print machine (SHINO I; SHINO, China; nozzle diameter = 0.3 mm, thickness = 0.1 mm). Volunteers wearing splints with landmarks [14] performed mandibular border movements, including maximal opening, closing, protrusion, retrusion, and lateral movements to the left and right sides. The movement trajectory was measured at 120 Hz using the mandibular movement recording system PN300 with 0.01mm error (Fig. 1 (A)) [37].

Using the original positional relationship between the maxillary and mandibular models from the oral scanner, the mandibular model and mandibular movement trajectory were registered in the same coordinate system (Fig. 1 (B)). The mandible moved according to the trajectory coordinates and the condylar positions at different times were recorded in Geomagic Studio. These were then merged into a single model to obtain the condylar movement envelope surface formed by the border movements (Fig. 1 (C)).

2.3. Simplification of the envelope surface to a two-dimensional curve

The envelope surfaces were shaped as two peaks and the second peak was lower. The depression between the two peaks was below the articular tubercle. The condyle moves forward and downward from the ICP and crosses the lowest point of the articular tubercle and moves slightly upward, forming the two peaks [39]. Based on the similar morphology of the envelope surface and the formation process, we simplified it in the sagittal dimension. A line was drawn at the middle points of the two peaks (Fig. 1 (E)). The envelope surface was divided into halves by a plane passing through the line and perpendicular to the Frankfurt horizontal plane (FH plane). A curve was extracted from half of the envelope surface, called the sagittal section curve (Fig. 1 (F)). The points reflecting the main characteristics of the curve were selected and named feature points (Fig. 1 (G)).

2.4. Cephalometric parameters

The CBCT was imported into ProPlan CMF 3.0 and cephalometric measurements were obtained. The 3D cephalometric landmarks and morphological parameters are shown in Table 1 and Fig. 2. SPSS Statistics 24.0 software (IBM Corp., Armonk, NY, USA) was used for data analyses.

3. Results

3.1. Basic information of the research object

Based on the inclusion criteria, 34 participants were included (mean age: 25.68 ± 2.71 years), including nine males (mean age: 25.48 ± 2.95 years) and 25 females (mean age: 26.22 ± 1.92 years).

3.2. Classification based on the morphology of the envelope surface

The envelope surfaces were classified into two types. Type 1 (typical) showed an obvious second peak after the first peak, while type 2 (atypical) showed a relatively flat second peak.

A new coordinate system was positioned as follows: (1) Determine the FH plane by the two orbitale points and the midpoint of porion points. (2) Determine a plane (plane 1) passing the middle points of the two peaks and perpendicular to the FH plane to divide the envelope surface into halves. (3) The simplified sagittal section curve was extracted according to 2.3. The line formed by the intersection of plane 1 and the FH plane was the X-axis, and the Y-axis was defined as perpendicular to the X-axis in plane 1. The first extreme point of the curve was the origin (point 1), the second extreme point was the lowest point between the two peaks (point 2), and the third extreme point was the highest point of the second peak (point 3). The height of the first peak was taken as the absolute
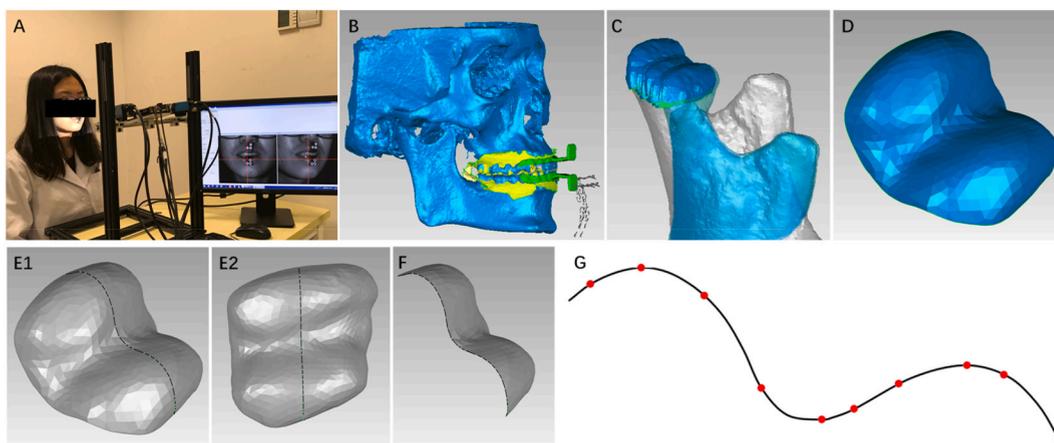

Fig. 1. (A) Mandibular trajectory recording [38]. Volunteers wearing splints with landmarks performed mandibular border movements, including maximal opening, closing, protrusion, retrusion, and lateral movements to the left and right sides.
(B) The registered model. Blue parts represent the reconstructed maxillary and mandibular models, yellow parts represent the dentition models, green parts represent the splints, and the points data indicates the trajectory.
(C) The mandible moving according to the trajectory; right condylar movement is shown.
(D) The condyle movement envelope surface.
(E) The position of the sagittal section curve.
(F) The morphology of half of the envelope surface and the extracted curve.
(G) The feature points and the curve. (For interpretation of the references to colour in this figure legend, the reader is referred to the Web version of this article.)

Table 1

Three-dimensional cephalometric landmarks and morphological parameters.

| Landmarks	Definition
Nasion (N)	Point at bridge of the nose where the frontal and nasal bones of the skull meet
Sella (S)	Saddle-shaped, hollowed extension of the sphenoid bone
Orbitale (O)	Lowest point on the lower edge of the cranial orbit
Porion (P)	Highest point on the external auditory canal
Condylion (Co)	Highest point of the condyle
Subspinale(A)	Deepest point at the midline of the bony concavity below the anterior nasal spine
Supramentale(B)	Most posterior midline point above the chin on the mandible, between the infradentate and pogonion
Menton (Me)	Lowest point of the mandibular symphysis
Gonion (Go)	Midpoint of the mandibular angle between the ramus and corpus mandibulae
FH plane	A plane determined by the porions bilaterally and the midpoint of the orbitales
Morphological parameters	
SNA	Angle formed by sella-nasion-point A
SNB	Angle formed by sella-nasion-point B
Mandibular width	Distance between Go on the left and right sides
Mandibular body length (L/R)	Distance between Go and Me
Menton angle	Angle between Na–Me and FH plane
Mandibular body angle	Angle between Go-Me and FH plane
Ramus height (L/R)	Distance between Co and Go
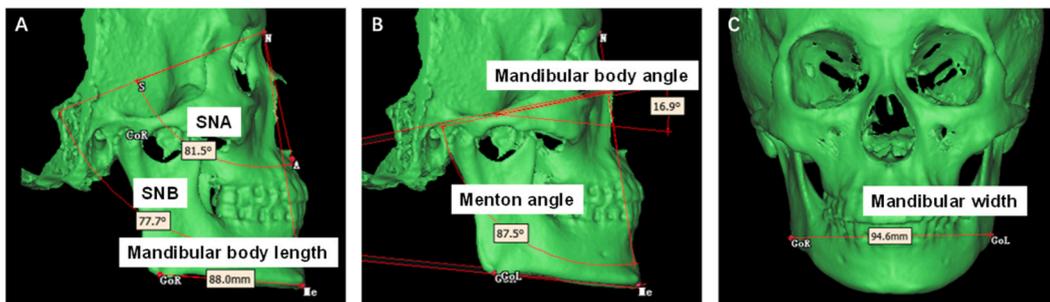
Fig. 2. (A) SNA, SNB, and mandibular body length. (B) Mandibular body and menton angles. (C) Mandibular width.
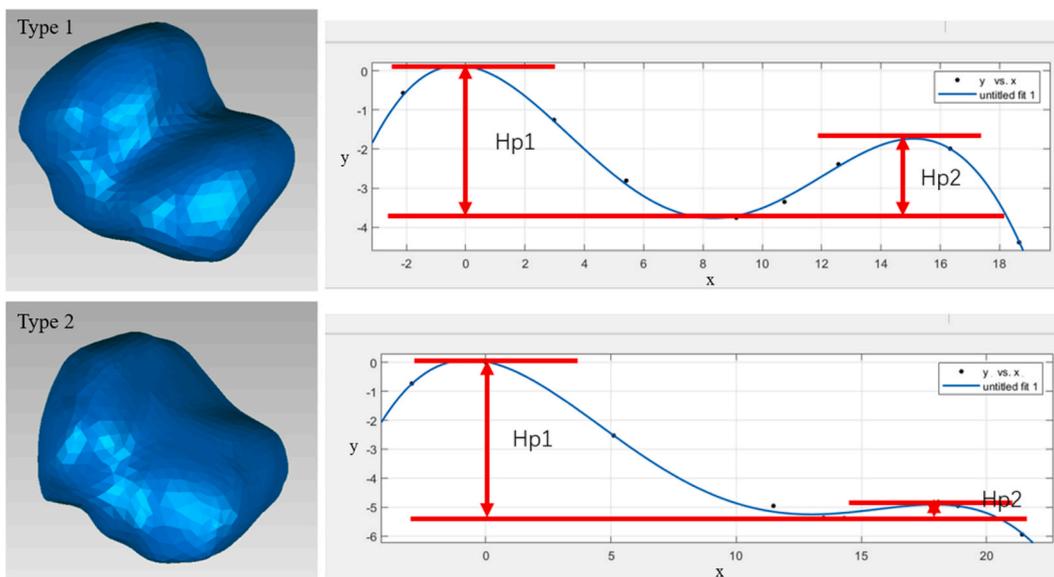

Fig. 3. The shape of the envelop surface and sagittal section curve fitting for types 1 and 2.

difference between the Y coordinates of points 1 and 2; the height of the second peak was defined by points 2 and 3. In the typical type, the height of the second peak was (H_{p2}) $\geq 1/3 \times$ height of the first peak (H_{p1}); while in the atypical type, the height was $H_{p2} < 1/3 \times H_{p1}$ (Fig. 3). The envelope surfaces were quantitatively divided into two types using this method. Based on this classification, 18 (14 females and 4 males) and 16 (11 females and 5 males) cases were classified as typical and atypical, respectively.

The classification was based on the envelope surface morphology and the shape of the sagittal curve. The qualitative classification was based on the envelope surface morphology, while the quantitative classification was based on the feature point coordinates. The aim was to group envelope surfaces according to their morphology to facilitate data processing.

3.3. Cephalometric analysis and classification based on facial parameters

The data for mandibular body length and ramus height were divided into the left and right sides. An independent sample *t*-test was performed for the left and right sides, but there was no statistical difference between the two sides (p = 0.357 and 0.232 for mandibular body length and ramus height, respectively). This indicated that the left and right sides were symmetrical for the participants of this study. The mean mandibular body length (85.2 ± 4.4 mm) and mean ramus height ($62. \pm 5.4$ mm) were used for subsequent tests. An independent sample *t*-test was performed for the data based on sex (Table 2). There was a statistically significant difference in the mandibular body length between sexes, reflecting the size of the mandible.

The maximum straight-line distances of the trajectory were measured. An independent sample *t*-test was performed for the left and right maximum lateral movements, and there was no statistically significant difference (p = 0.763).

The SNA and SNB values, which reflect the relative sagittal positions of the maxilla and mandible to the skull base, respectively, were significantly different between the two types (p < 0.05). Both SNA and SNB for type 2 were significantly greater than those for type 1. There were no statistically significant differences in the remaining parameters. An independent sample *t*-test was performed to evaluate the statistically significant differences in facial parameters between males and females (Table 3). SNA was significantly greater for the type 2 group compared to type 1 among female participants. Among male participants, the mandibular body length was significantly smaller for type 1 than for type 2. There were no statistically significant differences in the remaining parameters.

3.4. Classification based on the envelope surface's morphology and facial parameters

Based on the morphological differences in the envelope surfaces and cephalometric differences between the sexes, the envelope surfaces were divided into four categories: female typical, male typical, female atypical, and male atypical.

3.5. Curve fitting and functional expression

The sagittal section curves were imported into MATLAB (MathWorks, Natick, MA, USA) and displayed as spatial point coordinates (X, Y, and Z). According to Rodrigues' rotation formula, function (1), the spatial point coordinates were transformed into plane point coordinates (X and Y) in MATLAB.

$$e^{\hat{\omega}\theta} = I + \hat{\omega} sin\,\theta + \hat{\omega}^2 (1 - cos\,\theta) \tag{1}$$

The vertex of the first peak was defined as the original position. The transformed curve was rotated clockwise or counterclockwise to parallel the X-axis to the FH plane. The feature points of the curve, including the starting and extreme points, were marked as reference points for curve fitting. Several function forms were used to fit the feature points, including the Lagrange, polynomial, and Fourier functions. According to the adjusted R-square and the complexity of the function, the second-order Fourier function, containing six coefficients, was chosen to fit the envelope curves. The expression of the mathematical model achieved good fitting effects, and the adjusted R-square was 0.95–0.99. The feature points on these curves could use a second-order Fourier function as shown in function (2).

$$f(x) = a0 + a1 \times cos(x \times w) + b1 \times sin(x \times w) + a2 \times cos(2 \times x \times w) + b2 \times sin(2 \times x \times w) \tag{2}$$

3.6. Mapping relationship expressions

Curve-fitting could be performed using a second-order Fourier function based on the selected feature points for each sagittal curve.

Table 2
Cephalometric parameter analysis and independent sample *t*-test for sex, the values are mean $\pm$ SD.

Morphological parameter	Total	Female	Male	p
SNA(°)	82.4 ± 4.5	82.3 ± 4.7	82.6 ± 4.3	0.868
SNB(°)	79.5 ± 4.3	79.3 ± 4.6	80.0 ± 3.5	0.715
Mandibular width (mm)	100.2 ± 8.5	96.7 ± 6.7	109.8 ± 5.1	0.683
Menton angle (mm)	86.5 ± 2.5	86.1 ± 2.7	87.5 ± 1.5	0.138
Mandibular body angle (mm)	23.1 ± 4.9	23.6 ± 4.7	21.6 ± 5.4	0.302
Ramus height (mm)	62.3 ± 5.4	60.0 ± 3.6	68.7 ± 4.3	<0.001
Mandibular body length (mm)	85.2 ± 4.4	83.7 ± 3.9	89.2 ± 2.9	<0.001

Table 3

Independent t-test for cephalometric parameters for the two types, the values are mean $\pm$ SD.

Morphological parameter	Total			Female			Male		
	Type 1	Type 2	p	Type 1	Type 2	p	Type 1	Type 2	p
SNA (°)	80.4 $\pm$ 3.7	84.6 $\pm$ 4.4	0.004	80.1 $\pm$ 4.1	85.0 $\pm$ 4.1	0.007	81.1 $\pm$ 2.2	83.8 $\pm$ 5.47	0.391
SNB (°)	78.0 $\pm$ 3.3	81.2 $\pm$ 4.7	0.023	77.9 $\pm$ 3.6	81.2 $\pm$ 5.1	0.068	78.3 $\pm$ 2.1	81.3 $\pm$ 4.1	0.359
Menton angle (°)	86.3 $\pm$ 2.5	86.6 $\pm$ 2.5	0.785	86.2 $\pm$ 2.8	85.9 $\pm$ 2.6	0.765	86.8 $\pm$ 0.8	88.1 $\pm$ 1.8	0.222
Mandibular body angle (°)	23.4 $\pm$ 5.5	22.8 $\pm$ 4.3	0.726	23.8 $\pm$ 5.5	23.5 $\pm$ 3.6	0.874	22.1 $\pm$ 6.0	21.3 $\pm$ 5.6	0.852
Mandibular width (mm)	98.6 $\pm$ 7.7	101.9 $\pm$ 9.2	0.268	95.9 $\pm$ 6.0	97.8 $\pm$ 7.6	0.510	108.2 $\pm$ 5.6	111.0 $\pm$ 4.9	0.443
Ramus height (mm)	62.1 $\pm$ 5.1	62.5 $\pm$ 5.9	0.811	60.1 $\pm$ 3.5	59.8 $\pm$ 3.9	0.836	69.0 $\pm$ 4.0	68.5 $\pm$ 5.0	0.895
Mandibular body length (mm)	84.2 $\pm$ 3.3	86.2 $\pm$ 5.2	0.178	83.4 $\pm$ 3.3	84.0 $\pm$ 4.7	0.705	86.9 $\pm$ 1.5	91.1 $\pm$ 2.2	0.015

We standardized the point coordinates in each group to obtain the average feature points and performed curve-fitting using a second-order Fourier function to obtain the average function.

Since the condyle morphology is usually abnormal or difficult to identify in patients who need TMJ reconstruction, facial morphological measurements were performed without condylar landmarks. We selected six face-type parameters (SNA, SNB, mandibular width, mandibular body length, menton angle, and mandibular body angle) based on previous studies, and calculated their average values [31–34,40–43]. The criteria for the six parameters were also obtained from previous studies. Pearson's correlation analysis showed that the correlations between SNB and lateral mandibular movements, between mandibular body length and anteroposterior condylar diameter, and between mandibular body angle and envelope surface width were −0.403, 0.367, and −0.365, respectively.

These morphological parameters constituted vector A, while the six coefficients of the second-order Fourier curve constituted vector B. Since the morphological parameters were related to condylar movement, a sixth-order matrix M was used to represent the mapping relationship between A and B (functions (3) and (4)).

$$B = MA \tag{3}$$

$$
\begin{bmatrix} a0 \\ a1 \\ b1 \\ a2 \\ b2 \\ w \end{bmatrix} =
\begin{bmatrix} m_{11} & \cdots & m_{16} \\ \vdots & \ddots & \vdots \\ m_{61} & \cdots & m_{66} \end{bmatrix}
\begin{bmatrix} \text{SNA} \\ \text{SNB} \\ \text{Mandibular width} \\ \text{Mandibular body length} \\ \text{Menton angle} \\ \text{Mandibular body angle} \end{bmatrix} \tag{4}
$$

3.7. Envelope surface prediction

3.7.1. Individual sagittal curve prediction

The matrix M calculated using A and B represents the mapping relationship between the morphology and the envelope surface sagittal section curve for each group. The curve function coefficients for an individual of a known type could be predicted using the individual's morphological parameters and the matrix M for the type.

An example using the vectors A (facial parameters) and B (function coefficients), and the calculated M for a female of type 1 is shown below.

$$A = [80.14\ 77.86\ 95.89\ 83.41\ 23.76\ 86.22]^T$$

$$B = [-2.166\ 0.7934\ 0.9846\ 1.418 - 0.6501\ 0.237]^T$$

$$
M = \begin{bmatrix}
-0.0047 & -0.0046 & -0.0057 & -0.0049 & -0.0014 & -0.0051 \\
0.0017 & 0.0017 & 0.0021 & 0.0018 & 0.0005 & 0.0019 \\
0.0022 & 0.0021 & 0.0026 & 0.0022 & 0.0006 & 0.0023 \\
0.0031 & 0.0030 & 0.0037 & 0.0032 & 0.0009 & 0.0033 \\
-0.0014 & -0.0014 & -0.0017 & -0.0015 & -0.0004 & -0.0015 \\
0.0005 & 0.0005 & 0.0006 & 0.0005 & 0.0002 & 0.0006
\end{bmatrix}
$$

For a female of type 1 with the morphological parameters of SNA = 80.3°, SNB = 75.4°, mandibular width = 90 mm, mandibular body length = 80 mm, menton angle = 83.9°, and mandibular body angle = 24.7°, A' = [80.3 75.4 90 80 83.9 24.7]^T). Therefore, the prediction parameters for the curve function would be as follows:

$$B' = MA' = [-2.0947\ 0.7673\ 0.9533\ 1.3713 - 0.6287\ 0.2292]^T \tag{5}$$

The parameters were substituted into function (2) to obtain the prediction curve. The original sagittal curve and the prediction curve for this individual are shown in Fig. 4 (A).

3.7.2. Envelope surface prediction

Based on the predicted sagittal section curves, we predicted the morphology of the envelope surfaces. The condyle model and half of the envelope surface were imported into SolidWorks (SolidWorks Corp., Waltham, MA, USA). The condylar model was translated using point coordinates on the predicted curve. The point coordinates were taken at 1-mm intervals from −2 mm to the apex of the second peak in the X-axis (Fig. 4(B)). The condylar models for all positions are shown in grey, while the actual envelope surface is shown in blue (Fig. 4(C)).

The condylar models for all positions were imported into 3-Matic (Materialise), and the outer surfaces of the models were obtained by wrapping, which was the preliminary envelope surface. The preliminary envelope surface model was imported into Geomagic Studio, and the predicted envelope was obtained by enlarging it by 2 mm in the direction of the inner and outer diameters of the condyle based on our previous research [44]. Deviation analysis for the predicted envelope surface using the actual envelope as reference was 0.9970 ± 0.2918 mm. An example of the deviation analysis is shown in Fig. 4 (D).

4. Discussion

Previous mandibular condylar process analyses have used condylar landmarks, but inconsistencies in the selection criteria for landmarks prevented the comparison of these results [12,13]. In addition, this method does not reflect the 3D shape of the condylar process. Koolstra et al. [45] first introduced the concept of envelope surface and studied the envelope surface of incisor movements to evaluate the effects of temporomandibular ligaments and passive tension of the muscles on the envelope. We developed a method to analyze condylar movements in the four dimensions using CBCT and movement data. The concept of envelope surface was first proposed in the studies of condylar movement [14,46]. Huang's method was used to further investigate this in the present study. In 34 healthy adults, the envelope surface showed two peaks, consistent with the Huang study [46]. The morphology of the two-peak was related to the condylar movement during mandibular border movements. When the mandible opens and protrudes from the ICP, the condyle moves forward and downward, forming the first peak. Thereafter, the condyle moves slightly upward, which forms the second peak.

In recent years, mathematical expressions have been increasingly used in medical research [10,38,47–53]. Shang et al. established the functional models for cleft palate patients [47], while Wellens applied these functions to analyze mandibular arch forms in mixed dentition patients with crowding [49]. The envelope surface reflects the outer 3D shape of the condylar movement. Although the geometric morphology of the envelope surfaces showed some similarities, there were still significant individual differences compared to the corneal surface [48,54] and semicircular canals [50]. Therefore, it is difficult to mathematically express the geometric morphology of envelope surfaces. In a study of mandibular movements, Shu et al. used different functions to analyze condylar trajectories [10], but the study used point landmarks instead of the 3D condyle and could not complete a single function to express the condylar trajectory. We simplified the 3D envelope surface into a sagittal section curve based on the morphology. The present study showed that a second-order Fourier function could realize the mathematical fitting, retaining the essential characteristics of the
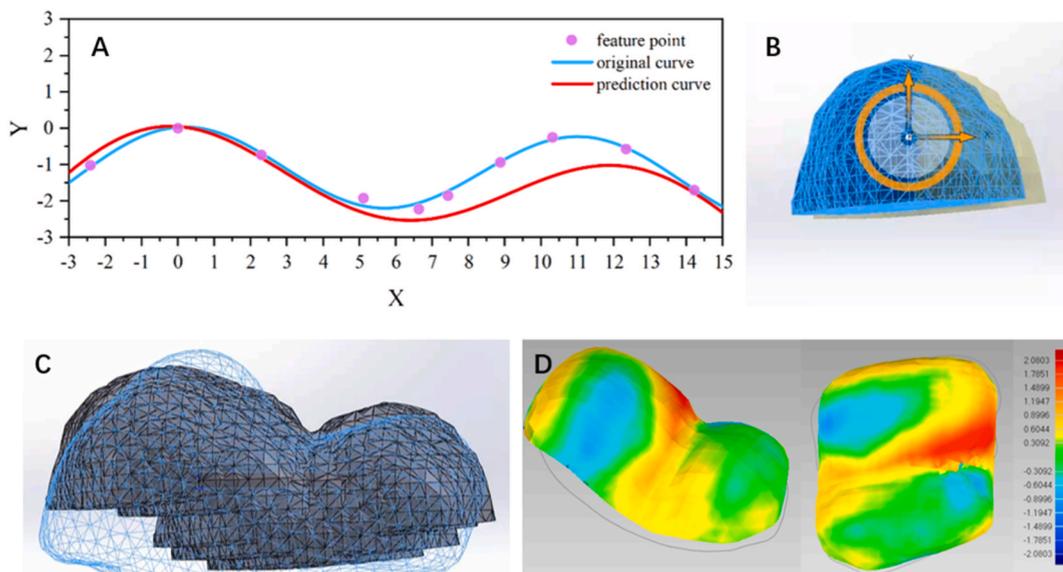

Fig. 4. (A) Original curve (blue), predicted curve (red), and feature points (purple).
(B) Translation of the condylar model.
(C) The actual envelope surface (blue) and the condyle models for all positions.
(D) Deviation analysis of the predicted and actual envelope surfaces. (For interpretation of the references to colour in this figure legend, the reader is referred to the Web version of this article.)

sagittal curve. In contrast with using points to record condylar trajectories, we focused on the 3D morphological characteristics of the condylar movement. After summarizing the morphological characteristics of the envelope surfaces, we simplified them to sagittal section curves and realized the mathematical expression for these curves. The fitted curve and associated parameters may be easier to use for pattern recognition for future artificial intelligence. Furthermore, mathematical formulas could provide clear functional information about the sagittal shape of the condylar envelope surfaces for subsequent analyses, such as machine learning.

TMJR is a biomechanical treatment option for end-stage TMD patients [20–22]. Most artificial TMJR systems use a ball-socket design, which cannot replicate the normal TMJ function. Ramos et al. [27] studied the effects of unilateral total TMJR on the contralateral joint, and suggested that placing an implant on one side affected the load distribution, particularly on the opposite side. Xu et al. [55] used the finite element method to analyze the mechanical responses of different prosthesis models, and found that the total TMJ prosthesis changed the biomechanical balance of the TMJ bilaterally. The articular head of the condylar component of the Melbourne prosthesis [56] has a circular and slightly flattened design to facilitate greater translation during mastication, while the fossa concavity is hemispherical to match the condylar head, aiming to allow condylar translation. Based on the finite element analysis of unilateral joint replacement, Pinheiro et al. [29] found that the movement distances of the prostheses during opening, protrusion, and lateral movements were greater than those for the contralateral natural joints. This suggests that any new TMJR design must consider the stability of condylar process during functional movements. Zhang et al. [57] analyzed the articular bone structure in 448 normal computed tomograms, and designed personalized prostheses similar to the bone structure. However, the personalized total joint prostheses showed asymmetric mandibular movements and limited lateral movements [58]. During 1–2 years of follow-up in patients who underwent unilateral TMJR using this system, 25% complained of discomfort due to excessive contralateral joint movements [59]. Our previous studies indicated that the 3D morphology of condylar movement may be used to design the artificial fossa [14,60]. The envelope surface may guide the movement of the condylar process. We also found that the downward angle of the envelope surface was not coincident with the posterior slope angle of the articular tubercle, indicating that the bony structure of the fossa could not be used as a guide for the movement of the artificial joint head in the absence of a disc [39]. Furthermore, it was also demonstrated that the condylar envelope surface could be used for the artificial fossa design [14,60]. Based on our previous studies, a more physiologically compatible TMJR system needs to be investigated, both geometrically and in terms of materials. The purpose of studying the envelope surface is to provide a foundation for the geometric design of the functional artificial joint fossa component, which may guide and support the movement of the joint head in the absence of the articular disc.

Patients with end-stage joint diseases, such as TMJ tumors and ankylosis, often have restricted mouth opening, which precludes the use of Huang's method to obtain the condylar motion envelope for artificial joint design [46]. Mandibular movement is closely related to the bone structure, muscles, and ligaments. The relationship between facial morphology and mandibular movements [31,34,42,61], and that between the 3D cephalometric parameters and condylar movements, have been investigated previously [32]. Facial morphology includes soft and hard tissues; the measurements for bones are more accurate and reproducible than those for soft tissues. Some previous studies have demonstrated that mandibular movement may be related to facial morphology. Therefore, the present study explored the relationship between facial morphology and the condylar envelope. Since the TMJ patients who require TMJR may lose reliable measurement landmarks due to factors, such as tumors and trauma, the present study selected six facial parameters, including SNA, SNB, mandibular body length, mandibular width, mandibular body angle, and menton angle. SNA and SNB reflect the sagittal anteroposterior relationship of the maxilla and mandible with the skull. Mandibular body length and width reflect the size of the mandible. The mandibular body angle reflects the relationship of the mandible with the FH plane, while the menton angle reflects the anteroposterior facial orientation relative to the FH plane. None of these parameters require joint-related measurement landmarks. Kim et al. investigated the mandibular movements and facial parameters obtained using 3D cephalometric measurements, and found that SNA, SNB, and mandibular body length correlated positively with the condylion [61]. Farella et al. investigated the relationship between vertical morphology and sagittal mandibular movement, and concluded that the opening-closing angle and mandibular body angle were inversely correlated [33]. The 3D cephalometric data for healthy adults in the present study agreed with those reported previously [61,62].

Zhang et al. [63] established a covariance matrix to describe the differences between sample and average crown models and to design personalized anatomical morphology for each tooth. Since the facial parameters and function expression parameters were two separate datasets and could be related, the matrix was used to express the mapping relationship between facial parameters and the envelope surface. The volunteers were divided into four groups according to sex and envelope morphology to achieve higher similarity within groups. We obtained the matrix mapping from facial morphology to the sagittal section curve using the calculated averages.

The preliminary predicted envelope surface model could be obtained by moving the condyle model along the curve. In a previous study, we found that the mediolateral diameter of the envelope surface was approximately 2 mm greater than the mediolateral diameter of the condyle [44]. Therefore, the preliminary model was enlarged to obtain the predicted envelope surface.

The deviation analysis indicated that the method could predict the envelope surfaces and the sagittal section curve could represent its main morphological characteristics to a certain extent, so the final predicted envelope surface may be obtained using the prediction curve. The method proposed in this study could predict individual envelope surfaces and provides a foundation for future research on envelope surfaces and artificial TMJR fossae.

In this study, the morphology of the condylar movement envelope surface was classified, simplified, and quantified to obtain a mathematical function expression. The matrix could represent the mapping from facial morphology to the condylar envelope surface of the healthy adults in northern China. The predicted sagittal section curve for the envelope surface was combined with the cephalometric parameters within groups through the matrix, which expressed the mapping relationship between facial parameters and the envelope surfaces. A combination of the predicted curve and the condylar model was used to predict the envelope surface. We further classified the envelope surfaces based on our previous study [14]. The mathematical function expression may be beneficial for the

integration of medicine and engineering in future studies of TMJ. The present study may provide a theoretical basis for understanding condylar movements and the geometric design of the artificial fossa component of TMJR systems.

The limitations of this study were the relatively small sample size and standard facial morphologies of the participants. We were unable to accurately determine the group of an individual using facial parameters alone, and the significance of each facial parameter requires further investigation. As this was an exploratory study using mathematical methods for envelope surface prediction, it may provide a basis for future TMJ studies. To verify the accuracy of this prediction method, further multicenter studies with larger samples are required. Furthermore, the envelope surface needs to be validated for use in designing the artificial fossa component matched to the artificial head. The feasibility and usability of the TMJR system need to be validated in future studies.

5. Conclusions

The envelope surfaces in healthy adults have a two-peak shape, which can be classified into type 1 ($H_{p2} \geq 1/3\ H_{p1}$) and type 2 ($H_{p2} < 1/3 \times H_{p1}$) according to the height ratio of these two peaks. There was a statistically significant difference in the mandibular body length between the sexes. SNA and SNB for type 2 were significantly greater than for type 1 ($p < 0.001$). Therefore, the participants were divided into four groups based on sex and envelope surface morphology.

The second-order Fourier function containing six coefficients could be used to describe the sagittal curve mathematically with the adjusted R-square ≥ 0.95. The function can be predicted based on the facial morphology using matrix mapping from cephalometric parameters. Based on the predicted curve and condylar process model, individualized envelope surfaces can be predicted. Deviation analysis for the predicted envelope surface using the actual envelope as a reference was carried out (root mean square = 0.9970 mm $\pm$ 0.2918 mm).

This method provides the foundation for future research and development in the medical and engineering fields. It may be used to design individualized geometric functional surfaces of the artificial fossa components of TMJR systems. This would support the movement of the joint head in the absence of the articular disc to achieve physiological mandibular movements.

Author contribution statement

Kenan CHEN: Conceived and designed the experiments; Performed the experiments; Analyzed and interpreted the data; Wrote the paper. Zhehao zhang: Conceived and designed the experiments; Contributed materials, analysis tools; editing the paper. Xiangliang Xu: Conceived and designed the experiments; Contributed reagents, materials, analysis tools or data. Junqi Jiang; Junlin Wang; Jing Wang: Performed the experiments. Yuchun Sun; Chuanbin Guo: Contributed reagents, materials, analysis tools or data.

Data availability statement

Data will be made available on request.

Declaration of competing interest

The authors declare that they have no known competing financial interests or personal relationships that could have appeared to influence the work reported in this paper.

Acknowledgments

References

[1] J. Fanghänel, T. Gedrange, On the development, morphology and function of the temporomandibular joint in the light of the orofacial system, Annals of anatomy = Anatomischer Anzeiger : official organ of the Anatomische Gesellschaft 189 (2007) 314–319, https://doi.org/10.1016/j.aanat.2007.02.024.

[2] E. Baltali, K.D. Zhao, M.F. Koff, E. Durmuş, K.N. An, E.E. Keller, A method for quantifying condylar motion in patients with osteoarthritis using an electromagnetic tracking device and computed tomography imaging, J. Oral Maxillofac. Surg. 66 (2008) 848–857, https://doi.org/10.1016/j.joms.2008.01.021.

[3] R.M. Andrade, L.R. Guimarães, A.P. Ribeiro, A. Pasqual Marques, O. Crivello Jr., B.K. Gonçalves de Carvalho, S.M. Amado João, Reliability in mandibular movement evaluation using photogrammetry in patients with temporomandibular disorders, J. Manipulative Physiol. Therapeut. 42 (2019) 267–275, https://doi.org/10.1016/j.jmpt.2018.11.008.

[4] C.C. Chen, C.C. Lin, H.P. Hsieh, Y.C. Fu, Y.J. Chen, T.W. Lu, In vivo three-dimensional mandibular kinematics and functional point trajectories during temporomandibular activities using 3d fluoroscopy, Dentomaxillofacial Radiol. 50 (2021), 20190464, https://doi.org/10.1259/dmfr.20190464.

[5] M.F. Lezcano, F.J. Dias, P. Chuhuaicura, P. Navarro, R. Fuentes, Symmetry of mandibular movements: a 3D electromagnetic articulography technique applied on asymptomatic participants, J. Prosthet. Dent 125 (2021) 746–752, https://doi.org/10.1016/j.prosdent.2020.01.020.

[6] J.E. Kim, J.H. Park, H.S. Moon, J.S. Shim, Erratum to "Complete assessment of occlusal dynamics and establishment of a digital workflow by using target tracking with a three-dimensional facial scanner" [J Prosthodont Res (2019) 120-124], J Prosthodont Res 63 (2019) 387, https://doi.org/10.1016/j.jpor.2019.03.003.

[7] S. Krohn, A.A. Joseph, D. Voit, T. Michaelis, K.D. Merboldt, R. Buergers, J. Frahm, Multi-slice real-time MRI of temporomandibular joint dynamics, Dentomaxillofacial Radiol. 48 (2019), 20180162, https://doi.org/10.1259/dmfr.20180162.

[8] D. Soydan Çabuk, M. Etöz, E. Akgün İ, S. Doğan, E. Öztürk, A. Coşgunarslan, The evaluation of lateral pterygoid signal intensity changes related to temporomandibular joint anterior disc displacement, Oral Radiol. (2020), https://doi.org/10.1007/s11282-020-00427-0.

[9] D.V. da Cunha, V.V. Degan, M. Vedovello Filho, D.P. Bellomo Jr., M.R. Silva, D.A. Furtado, A.O. Andrade, S.T. Milagre, A.A. Pereira, Real-time three-dimensional jaw tracking in temporomandibular disorders, J. Oral Rehabil. 44 (2017) 580–588, https://doi.org/10.1111/joor.12521.

[10] J. Shu, H. Ma, X. Xiong, B. Shao, T. Zheng, Y. Liu, Z. Liu, Mathematical analysis of the condylar trajectories in asymptomatic subjects during mandibular motions, Med. Biol. Eng. Comput. 59 (2021) 901–911, https://doi.org/10.1007/s11517-021-02346-6.

[11] Y. Feng, J. Shu, Y. Liu, T. Zheng, B. Shao, Z. Liu, Biomechanical analysis of temporomandibular joints during mandibular protrusion and retraction motions: a 3d finite element simulation, Comput. Methods Progr. Biomed. 208 (2021), 106299, https://doi.org/10.1016/j.cmpb.2021.106299.

[12] K. Ueda, Three-dimensional analysis for prediction and assessment of mandibular movement in orthognathic surgery in the ramus, J. Maxillofac. Surg. 11 (1983) 216–226, https://doi.org/10.1016/s0301-0503(83)80052-6.

[13] A. Zwijnenburg, C.C.E.J. Megens, M. Naeije, Influence of choice of reference point on the condylar movement paths during mandibular movements, J. Oral Rehabil. 23 (1996) 832–837, https://doi.org/10.1111/j.1365-2842.1996.tb00841.x.

[14] C. Huang, X.L. Xu, L.L. Li, Y.C. Sun, C.B. Guo, A study on reconstruction of the four-dimensional movement model and envelope surface of condyle in normal adults, Br. J. Oral Maxillofac. Surg. (2021), https://doi.org/10.1016/j.bjoms.2021.08.006.

[15] E. Schiffman, R. Ohrbach, E. Truelove, J. Look, G. Anderson, J.P. Goulet, T. List, P. Svensson, Y. Gonzalez, F. Lobbezoo, et al., Diagnostic criteria for temporomandibular disorders (DC/TMD) for clinical and research applications: recommendations of the international RDC/TMD consortium network* and orofacial pain special interest group†, Journal of oral & facial pain and headache 28 (2014) 6–27, https://doi.org/10.11607/jop.1151.

[16] T. List, R.H. Jensen, Temporomandibular disorders: old ideas and new concepts, Cephalalgia : an international journal of headache 37 (2017) 692–704, https://doi.org/10.1177/0333102416686302.

[17] T.M. Acri, K. Shin, D. Seol, N.Z. Laird, I. Song, S.M. Geary, J.L. Chakka, J.A. Martin, A.K. Salem, Tissue engineering for the temporomandibular joint, Advanced healthcare materials 8 (2019), e1801236, https://doi.org/10.1002/adhm.201801236.

[18] E.M. Ferneini, Temporomandibular joint disorders (TMD), J. Oral Maxillofac. Surg. 79 (2021) 2171–2172, https://doi.org/10.1016/j.joms.2021.07.008.

[19] B.J. Bielajew, R.P. Donahue, M.G. Espinosa, B. Arzi, D. Wang, D.C. Hatcher, N.K. Paschos, M.E.K. Wong, J.C. Hu, K.A. Athanasiou, Knee orthopedics as a template for the temporomandibular joint. Cell reports, Medicine 2 (2021), 100241, https://doi.org/10.1016/j.xcrm.2021.100241.

[20] L. Zou, D. He, C. Yang, C. Lu, J. Zhao, H. Zhu, Preliminary study of standard artificial temporomandibular joint replacement with preservation of muscle attachment, J. Oral Maxillofac. Surg. 79 (2021) 1009–1018, https://doi.org/10.1016/j.joms.2020.12.012.

[21] M.T. Neuhaus, A.N. Zeller, P. Jehn, B. Lethaus, N.C. Gellrich, R.M. Zimmerer, Intraoperative real-time navigation and intraoperative three-dimensional imaging for patient-specific total temporomandibular joint replacement, Int. J. Oral Maxillofac. Surg. 50 (2021) 1342–1350, https://doi.org/10.1016/j.ijom.2021.02.020.

[22] B. Murdoch, J. Buchanan, J. Cliff, Temporomandibular joint replacement: a New Zealand perspective, Int. J. Oral Maxillofac. Surg. 43 (2014) 595–599, https://doi.org/10.1016/j.ijom.2013.11.004.

[23] Y. Balel, M.K. Tümer, A bibliometric analysis of international publication trends in total temporomandibular joint replacement research (1986-2020), J. Oral Maxillofac. Surg. 79 (2021), https://doi.org/10.1016/j.joms.2021.02.038, 1458.e1451-1458.e1412.

[24] A. Wojczyńska, C.S. Leiggener, M. Bredell, D.A. Ettlin, S. Erni, L.M. Gallo, V. Colombo, Alloplastic total temporomandibular joint replacements: do they perform like natural joints? Prospective cohort study with a historical control, Int. J. Oral Maxillofac. Surg. 45 (2016) 1213–1221, https://doi.org/10.1016/j.ijom.2016.04.022.

[25] N. Celebi, E.C. Rohner, J. Gateno, P.C. Noble, S.K. Ismaily, J.F. Teichgraeber, J.J. Xia, Development of a mandibular motion simulator for total joint replacement, J. Oral Maxillofac. Surg. 69 (2011) 66–79, https://doi.org/10.1016/j.joms.2010.05.085.

[26] C.S. Leiggener, S. Erni, L.M. Gallo, Novel approach to the study of jaw kinematics in an alloplastic TMJ reconstruction, Int. J. Oral Maxillofac. Surg. 41 (2012) 1041–1045, https://doi.org/10.1016/j.ijom.2012.06.014.

[27] A.M. Ramos, M. Mesnard, The stock alloplastic temporomandibular joint implant can influence the behavior of the opposite native joint: a numerical study, J. Cranio-Maxillo-Fac. Surg. 43 (2015) 1384–1391, https://doi.org/10.1016/j.jcms.2015.06.042.

[28] L.M. Wolford, L.G. Mercuri, E.D. Schneiderman, R. Movahed, W. Allen, Twenty-year follow-up study on a patient-fitted temporomandibular joint prosthesis: the Techmedica/TMJ Concepts device, J. Oral Maxillofac. Surg. 73 (2015) 952–960, https://doi.org/10.1016/j.joms.2014.10.032.

[29] M. Pinheiro, R. Willaert, A. Khan, A. Krairi, W. Van Paepegem, Biomechanical evaluation of the human mandible after temporomandibular joint replacement under different biting conditions, Sci. Rep. 11 (2021), 14034, https://doi.org/10.1038/s41598-021-93564-3.

[30] A. Ramos, M. Mesnard, Comparison of load transfers in TMJ replacement using a standard and a custom-made temporal component, J. Cranio-Maxillo-Fac. Surg. 42 (2014) 1766–1772, https://doi.org/10.1016/j.jcms.2014.06.012.

[31] T. Kataoka, N. Kawanabe, N. Shiraga, T. Hashimoto, T. Deguchi, S. Miyawaki, T. Takano-Yamamoto, T. Yamashiro, The influence of craniofacial morphology on mandibular border movements, Cranio : J. Cranio-Mandibular Pract. 31 (2013) 14–22, https://doi.org/10.1179/crn.2013.003.

[32] T. Fukui, M. Tsuruta, K. Murata, Y. Wakimoto, H. Tokiwa, Y. Kuwahara, Correlation between facial morphology, mouth opening ability, and condylar movement during opening-closing jaw movements in female adults with normal occlusion, Eur. J. Orthod. 24 (2002) 327–336, https://doi.org/10.1093/ejo/24.4.327.

[33] M. Farella, G. Iodice, A. Michelotti, R. Leonardi, The relationship between vertical craniofacial morphology and the sagittal path of mandibular movements, J. Oral Rehabil. 32 (2005) 857–862, https://doi.org/10.1111/j.1365-2842.2005.01514.x.

[34] B. Ingervall, Variation of the range of movement of the mandible in relation to facial morphology in young adults, Scand. J. Dent. Res. 79 (1971) 133–140, https://doi.org/10.1111/j.1600-0722.1971.tb02003.x.

[35] D.S. Kim, K.H. Huh, S.S. Lee, M.S. Heo, S.C. Choi, S.J. Hwang, W.J. Yi, The relationship between the changes in three-dimensional facial morphology and mandibular movement after orthognathic surgery, J. Cranio-Maxillo-Fac. Surg. 41 (2013) 686–693, https://doi.org/10.1016/j.jcms.2013.01.011.

[36] D. Wang, H. Fu, R. Zeng, X. Yang, Changes of mandibular movement tracings after the correction of mandibular protrusion by bilateral sagittal split ramus osteotomy, J. Oral Maxillofac. Surg. 67 (2009) 2238–2244, https://doi.org/10.1016/j.joms.2009.04.075.

[37] T. Zhao, H. Yang, H. Sui, S.S. Salvi, Y. Wang, Y. Sun, Accuracy of a real-time, computerized, binocular, three-dimensional trajectory-tracking device for recording functional mandibular movements, PLoS One 11 (2016), e0163934, https://doi.org/10.1371/journal.pone.0163934.

[38] D. Schurzig, M.E. Timm, G.J. Lexow, O. Majdani, T. Lenarz, T.S. Rau, Cochlear helix and duct length identification - evaluation of different curve fitting techniques, Cochlear Implants Int. 19 (2018) 268–283, https://doi.org/10.1080/14670100.2018.1460025.

[39] K.N. Chen, J. Wang, J.P. Chen, J.L. Wang, Y.C. Sun, X.L. Xu, C.B. Guo, Comparative study of temporomandibular articular fossa bone surface and the envelope surface of the condyle movement, Chin. J. Dent. Res. : the official journal of the Scientific Section of the Chinese Stomatological Association (CSA) 25 (2022) 179–187, https://doi.org/10.3290/j.cjdr.b3317993.

[40] T. Muto, M. Kanazawa, The relationship between maximal jaw opening and size of skeleton: a cephalometric study, J. Oral Rehabil. 23 (1996) 22–24, https://doi.org/10.1111/j.1365-2842.1996.tb00807.x.

[41] R. Tabrizi, T. Karagah, E. Aliabadi, S.A. Hoseini, Does gum chewing increase the prevalence of temporomandibular disorders in individuals with gum chewing habits? J. Craniofac. Surg. 25 (2014) 1818–1821, https://doi.org/10.1097/scs.0000000000000993.

[42] B. Ingervall, Variation of the range of movement of the mandible in relation of facial morphology in children, Scand. J. Dent. Res. 78 (1970) 533–543.

[43] K.H. Travers, P.H. Buschang, H. Hayasaki, G.S. Throckmorton, Associations between incisor and mandibular condylar movements during maximum mouth opening in humans, Arch. Oral Biol. 45 (2000) 267–275, https://doi.org/10.1016/S0003-9969(99)00140-5.

[44] K.N. Chen, J.Q. Jiang, J.L. Wang, Y.C. Sun, C.B. Guo, X.L. Xu, Preliminary measurement and analysis of the condyle movement envelope surface parameters in healthy adults, Chin. J. Stomatol. 57 (2022) 1015–1021, https://doi.org/10.3760/cma.j.cn112144-20220630-00355.

[45] J.H. Koolstra, M. Naeije, T.M. van Eijden, The three-dimensional active envelope of jaw border movement and its determinants, J. Dent. Res. 80 (2001) 1908–1912, https://doi.org/10.1177/00220345010800100901.

[46] C. Huang, X. Xu, L. Li, Y. Sun, C. Guo, Study on the reconstruction of a four-dimensional movement model and the envelope surface of the condyle in normal adults, Br. J. Oral Maxillofac. Surg. 60 (2022) 884–889, https://doi.org/10.1016/j.bjoms.2021.08.006.

[47] F.F. Shang, X. Zhou, L. Ma, Application of mathematical function model in morphological description and classification of bone defect in cleft palate cases, Zhonghua Kou Qiang Yi Xue Za Zhi 54 (2019) 540–545, https://doi.org/10.3760/cma.j.issn.1002-0098.2019.08.008.

[48] Y. Di, M.Y. Li, T. Qiao, N. Lu, Edge detection and mathematic fitting for corneal surface with Matlab software, Int. J. Ophthalmol. 10 (2017) 336–342, https://doi.org/10.18240/ijo.2017.03.02.

[49] H. Wellens, Applicability of mathematical curve-fitting procedures to late mixed dentition patients with crowding: a clinical-experimental evaluation, Am. J. Orthod. Dentofacial Orthop. : official publication of the American Association of Orthodontists, its constituent societies, and the American Board of Orthodontics 131 (160) (2007) e117–e125, https://doi.org/10.1016/j.ajodo.2006.06.015.

[50] A.P. Bradshaw, I.S. Curthoys, M.J. Todd, J.S. Magnussen, D.S. Taubman, S.T. Aw, G.M. Halmagyi, A mathematical model of human semicircular canal geometry: a new basis for interpreting vestibular physiology, Journal of the Association for Research in Otolaryngology : JARO 11 (2010) 145–159, https://doi.org/10.1007/s10162-009-0195-6.

[51] V.F. Ferrario, C. Sforza, F. Randelli, A. Miani Jr., G. Pizzini, Femoral asymmetry in healthy adults: elliptic Fourier analysis using computerized tomographic scout views, Italian journal of anatomy and embryology = Archivio italiano di anatomia ed embriologia 103 (1998) 95–105.

[52] U. Fors, M.L. Ahlquist, R. Skagerwall, L.G.A. Edwall, G.A.T. Haegerstam, Relation between intradental nerve activity and estimated pain in man–a mathematical model, Pain 18 (1984) 397–408, https://doi.org/10.1016/0304-3959(84)90052-6.

[53] V.F. Ferrario, C. Sforza, M. Guazzi, G. Serrao, Elliptic Fourier analysis of mandibular shape, J. Craniofac. Genet. Dev. Biol. 16 (1996) 208–217.

[54] M.G. Shi, B. Wang, T.T. Shao, A study on the mathematical model of normal adult cornea, [Zhonghua yan ke za zhi] Chinese journal of ophthalmology 43 (2007) 694–697.

[55] X. Xu, J. Zhang, D. Luo, C. Guo, Q. Rong, Biomechanical comparison between the custom-made mandibular condyle prosthesis and total temporomandibular joint prosthesis in finite element analysis, Acta Bioeng. Biomech. 22 (2020) 151–160, https://doi.org/10.37190/ABB-01721-2020-03.

[56] D.C. Ackland, D. Robinson, M. Redhead, P.V.S. Lee, A. Moskaljuk, G. Dimitroulis, A personalized 3D-printed prosthetic joint replacement for the human temporomandibular joint: from implant design to implantation, J. Mech. Behav. Biomed. Mater. 69 (2017) 404–411, https://doi.org/10.1016/j.jmbbm.2017.01.048.

[57] L.Z. Zhang, S.S. Meng, D.M. He, Y.Z. Fu, T. Liu, F.Y. Wang, M.J. Dong, Y.S. Chang, Three-dimensional measurement and cluster analysis for determining the size ranges of Chinese temporomandibular joint replacement prosthesis, Medicine 95 (2016), e2897, https://doi.org/10.1097/md.0000000000002897.

[58] J. Zheng, X. Chen, W. Jiang, S. Zhang, M. Chen, C. Yang, An innovative total temporomandibular joint prosthesis with customized design and 3D printing additive fabrication: a prospective clinical study, J. Transl. Med. 17 (2019) 4, https://doi.org/10.1186/s12967-018-1759-1.

[59] L. Zou, J. Zhao, D. He, Preliminary clinical study of Chinese standard alloplastic temporomandibular joint prosthesis, J. Cranio-Maxillo-Fac. Surg. 47 (2019) 602–606, https://doi.org/10.1016/j.jcms.2019.01.045.

[60] X. Xu, D. Luo, C. Guo, Q. Rong, A custom-made temporomandibular joint prosthesis for fabrication by selective laser melting: finite element analysis, Med. Eng. Phys. 46 (2017) 1–11, https://doi.org/10.1016/j.medengphy.2017.04.012.

[61] D.S. Kim, S.C. Choi, S.S. Lee, M.S. Heo, K.H. Huh, S.J. Hwang, W.J. Yi, Correlation between 3-dimensional facial morphology and mandibular movement during maximum mouth opening and closing, Oral Surg. Oral Med. Oral Pathol. Oral Radiol. Endod. 110 (2010) 648–656, https://doi.org/10.1016/j.tripleo.2010.06.007.

[62] N. Zamora, J.M. Llamas, R. Cibrián, J.L. Gandia, V. Paredes, Cephalometric measurements from 3D reconstructed images compared with conventional 2D images, Angle Orthod. 81 (2011) 856–864, https://doi.org/10.2319/121210-717.1.

[63] C. Zhang, T. Liu, W. Liao, K. Zhang, Statistical reconstruction algorithm for restoring broken tooth surface based on occlusion spatial constraint, Jixie Gongcheng Xuebao 52 (2016) 165–174, https://doi.org/10.3901/JME.2016.01.165.